Summary of Research (Final Technical Report)

Investigating the Impacts of Changes in Land Cover and Land Management on Climate Using ACME

A Research Project Funded by the Office of Science (BER), US DOE, Award No: DOE-DE-SC0016323

Principal Investigator

Atul K Jain
Department of Atmospheric Science
1301 W Green St, Urbana, IL 61801

Phone: 217-333-2128
Email: jain1@illinois.edu

1. Major Goals of the Project

The overall objective of our ACME project is to advance the treatment of land disturbance, particularly land use and land cover changes (LULCCs) and land management practices, and couple it with ALM to fully explore the potential contribution of LULCC and land management practices to future emissions and mitigation opportunities, and terrestrial carbon sources and sinks, and climate change. To achieve this objective, we have incorporated the advances made by DOE in IAM and ESM modeling efforts and our research at UIUC in global land disturbance, carbon management, and socioeconomic research.

As part of this research, we have accomplished most of the tasks that we originally proposed, leading to the completion of the proposal. Under this grant, 12 journal articles, 2 book chapters, and 17 conference proceeding articles were published. All these articles acknowledged the financial support of this grant. In addition, this supported one Ph.D. student and 2 MS students.

As part of this research, we have accomplished the following tasks that we originally proposed.

2. Research Accomplishments

Task 1: Improving the LULCC in ACME/E3SM

Objective and Approach: This task aims to provide estimates of LULCCs (and underlying land-use conversions) in GCAM-ACME (hereafter E3SM) that are consistent with satellite and ground-based observations. We calibrated the historical LULCC data using the satellite and other ground-based data sets as part of this research. Our historical reconstruction data sets account for the changes in LULCC due to human activities and natural causes. We have analyzed the "bottom-up" LULCC data at country, regional and global scales to validate the "top-down" global LULCC estimates, and upscale local scale LULCC drivers to the global scale. The detailed biophysical and socioeconomic driver information at different spatial and temporal scales further helps improve the historical distribution of LULCC.

Accomplishments:

Task 1.1. Dynamic and drivers of LULCC at country and regional scales

Dynamic and drivers of LULCC at country scale: Bangladesh

The dominant LULC types in Bangladesh were agricultural land, forest, and waterbody (flowing and standing) in both 2000 and 2010. Overall, there was negligible change in the agricultural land and mangrove, whereas areas for shrub land (increased by 21.76%), barren land (increased by 41.06%), settlement (increased by 32.52%), and standing waterbody (increased by 8.63%) increased from 2000 to 2010; and area for forest (decreased by 8.90%), and flowing waterbody (decreased by 2.88%), decreased. Although the net change in agricultural land is almost negligible (increased by 0.13%, 153 km^2), but there is a drastic amount of gain and loss of agricultural land area (gain about 2003 km^2 and lost 1850 km^2) due to various land cover types, including flowing waterbody, barren land and shrubland. The forest was mainly replaced by shrubland, which increased by 21.77% (694 km^2). The decreasing rate of the forest was the greatest among all LULC types, indicating intensive deforestation activities.

The 40.90% net increased rate of barren land was the highest among all LULC types. The sources of increased barren land were mainly from agricultural land and flowing waterbody. The standing

waterbody area was increased by 8.58%, because a large area of agricultural land was converted to a standing waterbody (Fig. 1).

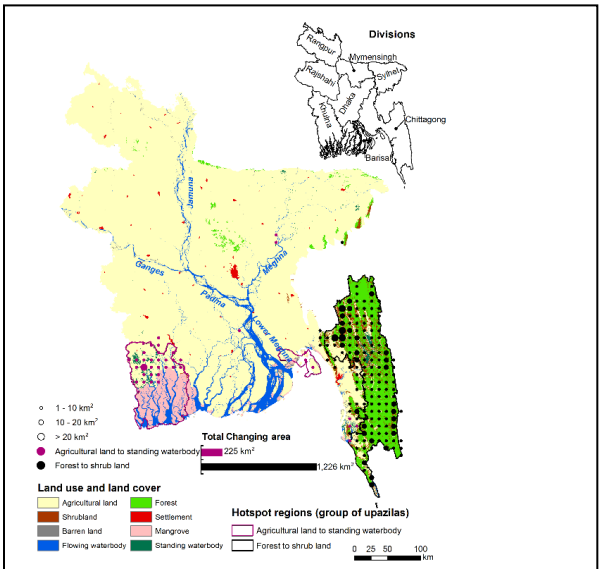

Fig. 1. Spatial pattern of land-use and land cover changes (LULCC) in Bangladesh between 2000 and 2010. The base map is the land-use and land cover map of 2000. The color and size of circles represent LULCC types and areas.

There are seven biophysical drivers out of the ten most predominant drivers for the conversion from forest to shrubland. Increasing rate and standard deviation of temperature are the two most important drivers, and both have positive impacts (positive relationship between drivers and LULCCs). The increasing rate of temperature in monsoon months also has a positive impact on this change. By contrast, four precipitation-related drivers, mean and standard deviation of precipitation both annually and in monsoon months, are all negatively correlated to the changes (negative relationship between drivers and LULCCs). Socioeconomic drivers, including increasing rates of rural and urban household sizes and rural household numbers, are negatively related to this change.

On the contrary, there are eight socioeconomic drivers and two biophysical drivers out of the ten most important drivers for the conversion from agricultural land to standing waterbody. Population, urban and rural household numbers and the increasing rate of rural household size have negative impacts. The increasing rate of urban household size is positively associated with this change. Meanwhile, the distance to major cities and connection ratio of electricity are negatively associated with the change, but the distance to major highways and other major roads is positively correlated to the change. The biophysical drivers, distance to rivers, and increasing precipitation rate in monsoon months all have negative impacts on the changes from agricultural land to standing waterbody (Fig. 2).

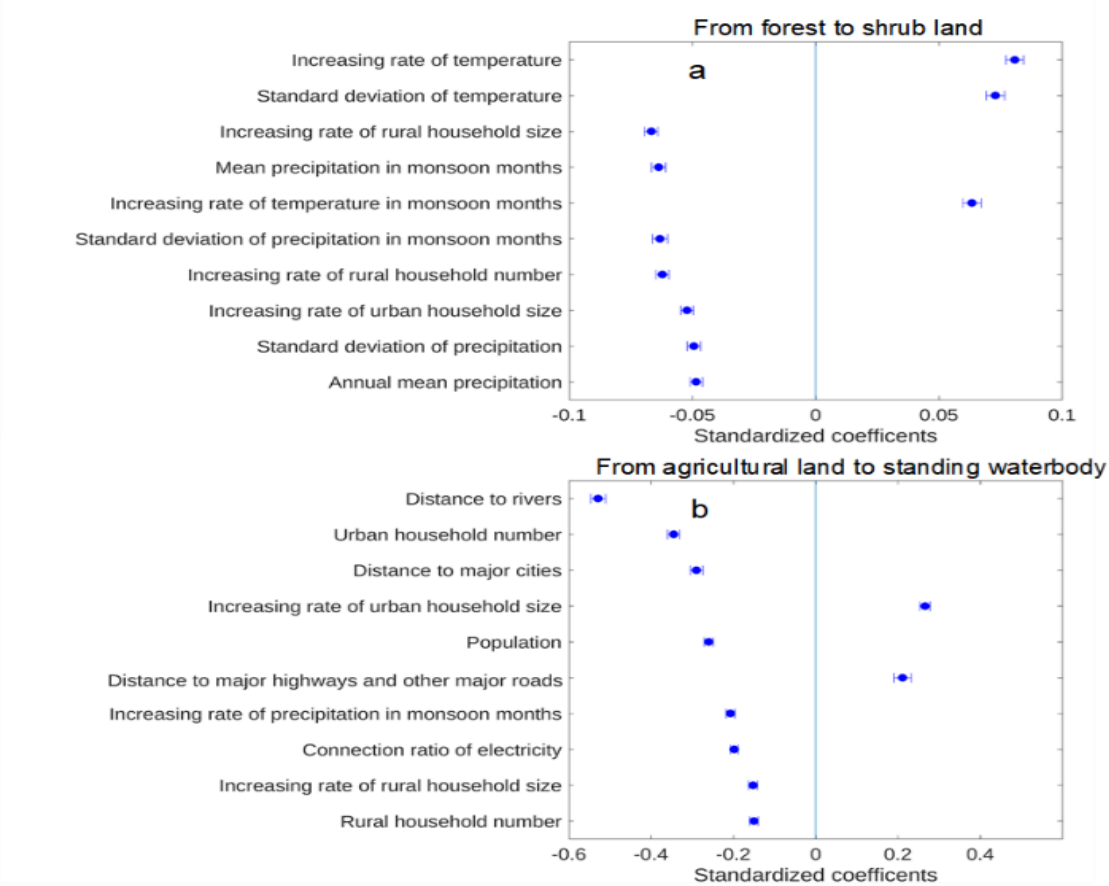

Fig. 2. Ten most prominent drivers for the land-use and land cover changes of: (a) forest to shrub land, and (b) agricultural land to standing waterbody from 2000 to 2010. Blue dots show the standardized coefficients, error bars show the 95% confidence interval. Standardized coefficients demonstrate the relative importance of each driver.

Dynamic and drivers of LULCC at regional scales: an example of South and Southeast Asia (SSEA) region

We took one of the hotspot regions of LULCCs in the world: South and Southeast Asia (SSEA) as the study area to further improve our global scale results. Based on the dynamics of forest and agricultural land from 1992 to 2015 from the Climate Change Initiative land cover data developed by the European Space Agency, we synthesized ~200 publications on LULCC drivers at different spatial scales in SSEA to identify the major drivers of these LULCC activities. For each major driver, we collected corresponding representative variables. A geographically weighted regression was employed to quantify the heterogeneous drivers of LULCC. We validated our results with national-level case studies in SSEA.

The case studies regarding the LULCC drivers of forest loss and gain spread in all countries and had diverse spatial scales, from village to national scale. The identified biophysical drivers included terrain, soil conditions, water, climate, fire/other natural disasters. The socioeconomic drivers mainly covered population, urbanization, livestock, market, plantation, agricultural expansion, mining and industry, accessibility/infrastructure, logging/fuelwood and poverty. Fire and terrain were the most frequently mentioned biophysical drivers of deforestation. In India and

Indonesia, the two countries with the largest area of forest, more studies suggested terrain and fire were major biophysical drivers. The synthesis also recognized the important socioeconomic drivers of deforestation as population, plantation, agricultural expansion, accessibility/infrastructure, and fuelwood/logging. India and Indonesia were also the most studied countries.

We found that socioeconomic drivers are more important than biophysical drivers for the conversion of forest to agricultural land in South Asia and maritime Southeast Asia. In contrast, biophysical drivers are more important than socioeconomic drivers for the conversion of agricultural land to the forest in maritime Southeast Asia and less important in South Asia. Both biophysical and socioeconomic drivers contribute approximately equally to both changes in the mainland Southeast Asia region (Fig. 3).

Drivers of LULCC at global scales

We employ the geographically weighted regression (GWR) model to uncover the spatiotemporally heterogeneous drivers of LULCC activities (for example, primary forest conversion to cropland and secondary forest) from 1900 - 2005. The GWR approach accounts for a distinct relationship between each LULCC grid cell and its driving variables by incorporating grid cells falling within a certain bandwidth of the target pixel. We are employing 31 biophysical variables and seven socioeconomic variables to analyze the historical LULCC drivers. Detailed variables and their sources can be found in Table 1.

We have implemented into SDAM: (1) Primary forest to cropland (Fig. 4) (2) primary forest to secondary forest (Fig. 5), (3) cropland to the secondary forest (Fig. 6), (4) primary forest to pastureland (results not discussed here), and (5) primary forest to urban land (results not discussed here). The study time period is 1900 – 2005. In order to simplify the results, here we discuss the results for average values for three different time periods: 1900 – 1919, 1940 – 1959, and 1980 – 2005.

Figs. 4 ~ 6 showed the spatiotemporally explicit drivers of the five LULCC activities. The first column in each figure showed the most dominant driver in each period. The values in column 1 referred to how many standard deviations the LULCC area will change per standard deviation increase in the drivers. The dominant drivers were the drivers with the greatest average absolute value among all 38 drivers for each period. The second columns in the figures are the dominant drivers in 283 Agro-Ecological Zones (AEZs, consistent with the GCAM AEZs) across the globe. The drivers in the second and third columns were aggregated into 11 categories for convenience. The third column showed the dominant drivers in each grid identified by the GWR model.

Drivers for the Conversions of Primary Forest to Cropland. The first column in Figure 4 showed that, in the earlier and middle periods of the 20th century, change in rural population density was the most dominant driver for the conversion from primary forest to cropland. The coefficients were mostly positive, indicating that in the regions where the rate of change (ROC) in rural population density was greater, the area of primary forest to cropland was bigger. In the area where the ROC in rural population was greater, food demands would also be larger. Humans exploited more cropland from primary forests to get more food. In 1980 – 2005, the change in urban population density became the most important driver with a negative correlation with the area of primary

forest conversion to cropland. The regions with higher ROC in urban population were usually located in big cities. There was less amount primary forest to be converted into cropland in such regions.

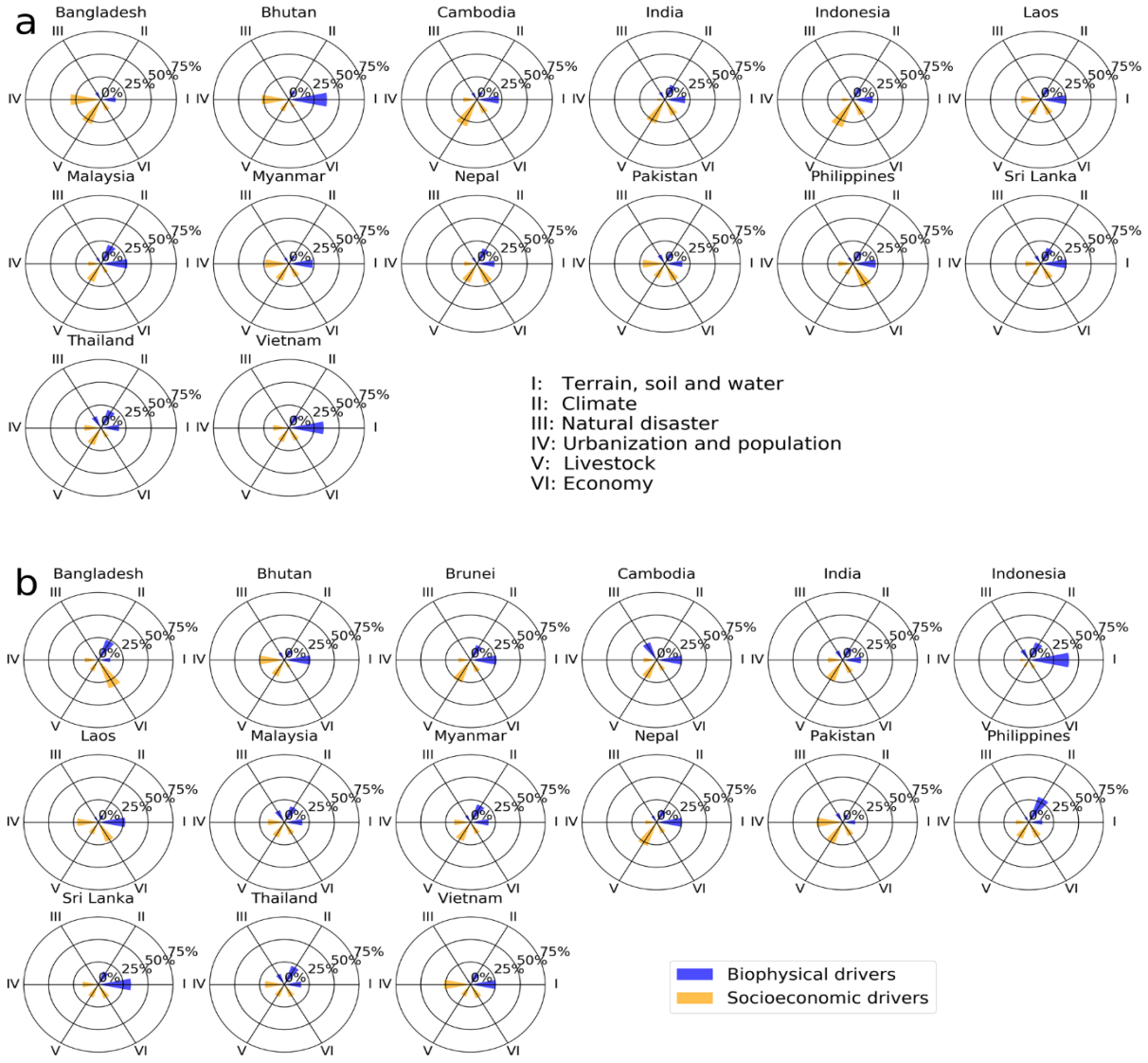

Fig. 3. The relative importance of different drivers for the conversions (a) from forest to agricultural land and (b) from agricultural land to forest in SSEA countries.

The second and third columns showed that rural population, precipitation, and market were the most widespread drivers. In 1900 - 1919 and 1940 - 1959, the rural population was dominant in North and South America and North Asia. The temperature was the dominant driver in Europe and North Africa. The urban area was most important in Central and South Africa. This pattern changed from 1980 – 2005. In this period, the market played a key role in a major part of South America and Central and East Africa. The area with the dominant driver from precipitation expanded.

Table 1. Biophysical and socioeconomic drivers of LULCC

Category	Data Variable	Description/Units	Spatial Characteristics	Period of Availability	Source
Terrain (1)	Elevation, Slope and Inclination Combined	Categorical Data classified into 9 gradient classes	5 minutes^ (lat/lon)	Constant with time	FAO/IIASA, 2010. Global Agro-ecological Zones (GAEZ v3.0). FAO, Rome, Italy and IIASA, Laxenburg, Austria. http://www.fao.org/nr/gaez/en/
Soil characters (5)	Soil fertility	Categorical Data classified into 7 gradient classes of land suitability for agriculture			
	Soil drainage				
	Chemical composition				
	Soil depth				
	Soil texture				
Temperature (6)	Temperature (T_a)	^oC	0.5 degrees (lat/lon)	1901-2009 (monthly)	Climatic Research Unit (CRU) TS 3.1 (updated estimates based on Mitchell and Jones, 2005)
	Daily Average Maximum Temperature (T_{max})				
Seasonal PET (4)	Potential Evapotranspiration	Millimeters			
Precipitation (7)	Precipitation				CRU TS 3.10.01#
Seasonal PDSI (4)	Palmer Drought Severity Index (PDSI)	No units	2.5 degrees@	1870-2010	Dai et al. (2011a,b)
Seasonal THI (4)	Temperature humidity index (THI)	^oC			
Socioeconomic Factors (7)	Urban/built-up land	% of grid-cell area	5 minutes^ (lat/lon)	10,000 BC – 2005 AD (decadal)%	Goldewijk et al. (2010)
	Urban Population	Inhabitants/km^2			
	Rural Population				
	Gross Domestic Product (GDP) per capita	Constant 1990 international (Geary-Khamis) dollars/person	National level	1 AD-2010	Bolt and Van Zanden (2013)
				(annually between 1800-2010)$	(The Maddison Project - http://www.ggdc.net/maddison/maddison-project/home.htm)
	Market Accessibility	No units	1 km^ (lat/lon)	~2005	Verburg et al. (2011)

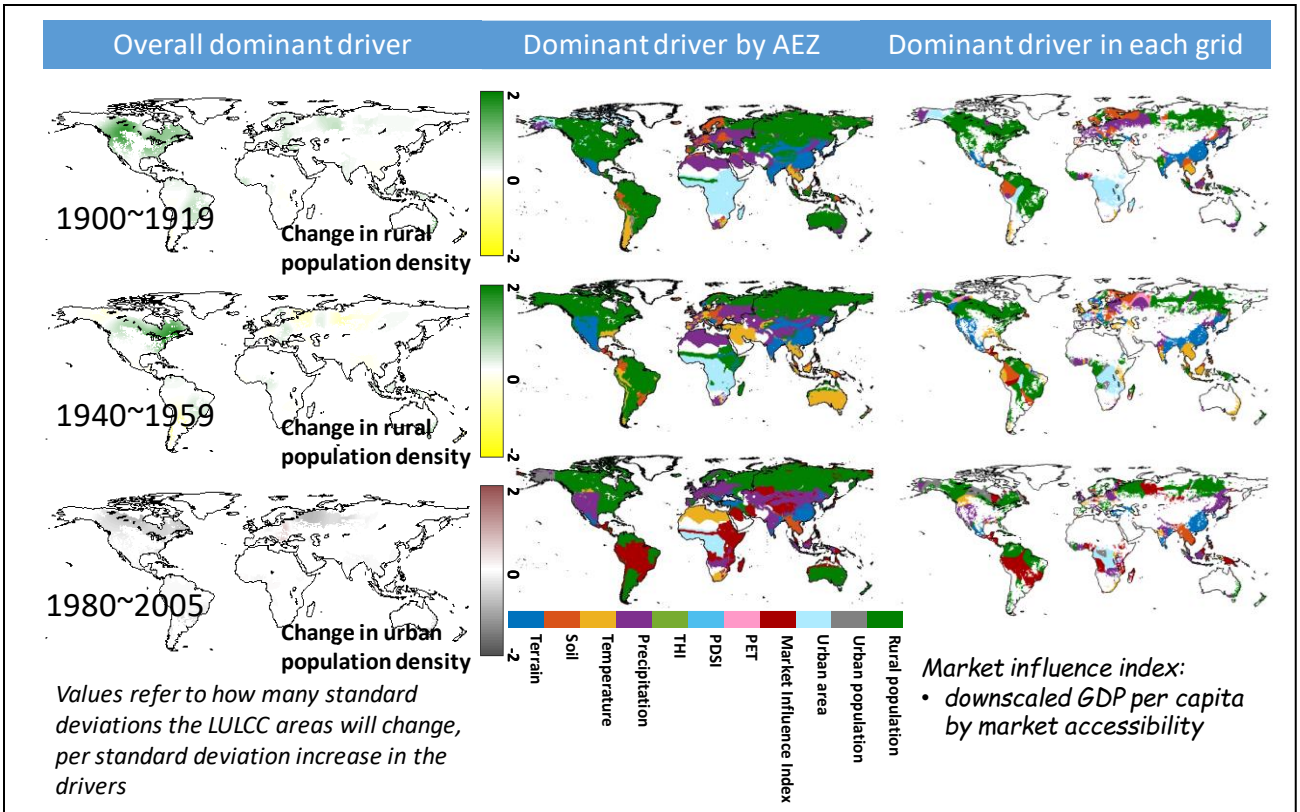

Figure 4. The overall dominant drivers of primary forest to cropland, dominant drivers for different AEZs and in each grid cell.

Drivers for the Conversions of Primary Forest to Secondary Forest. The first column in Figure 5 showed that, in the earlier 20th century, change in rural population density was also the most dominant driver for the conversion from primary forest to secondary forest. The coefficients were mostly negative, indicating that in the regions where the rate of change (ROC) in rural population density was greater, the primary forest area to the secondary forest was smaller. In these regions, people tended to exploit more cropland from primary forests rather than regrow the forest. In 1940 – 1959 and 1980 – 2005, mean fall precipitation and standard deviation of annual precipitation became the dominant drivers respectively, indicating the dominant drivers of primary forest to the second forest transferred from socioeconomic aspect to biophysical factor. In 1940 – 1959, the mean fall precipitation was the most important driver with a positive correlation with the primary forest conversion to secondary forest. In 1980 – 2005, the standard deviation of annual precipitation was the most important driver with a positive correlation with primary forest conversion to secondary forest. The primary forest would not directly convert to secondary forest. Usually, the primary forest would first convert into other land use or land cover types (for example, cropland). Then the land use or land cover types would further change into secondary forest. The regrowth of the forest required higher precipitation. Thus, in the regions with higher precipitation, the primary forest conversion to the secondary forest would be higher.

The second and third columns showed that precipitation, rural population, and temperature were the most widespread drivers. In 1900 – 1919, precipitation was dominant in North Asia and Europe. The rural population was the dominant driver in North America. 1940 – 1959 had a similar pattern

with 1900 -1919 in North Asia, North America, and Europe, but differed in East Asia, Australia, and South America, where the temperature became the dominant driver. The dominant drivers were considerably changed in 1980 – 2005. In this period, the rural population became dominant in North Asia. In North and South America, the rural population and precipitation dominated the conversion from primary to secondary forest.

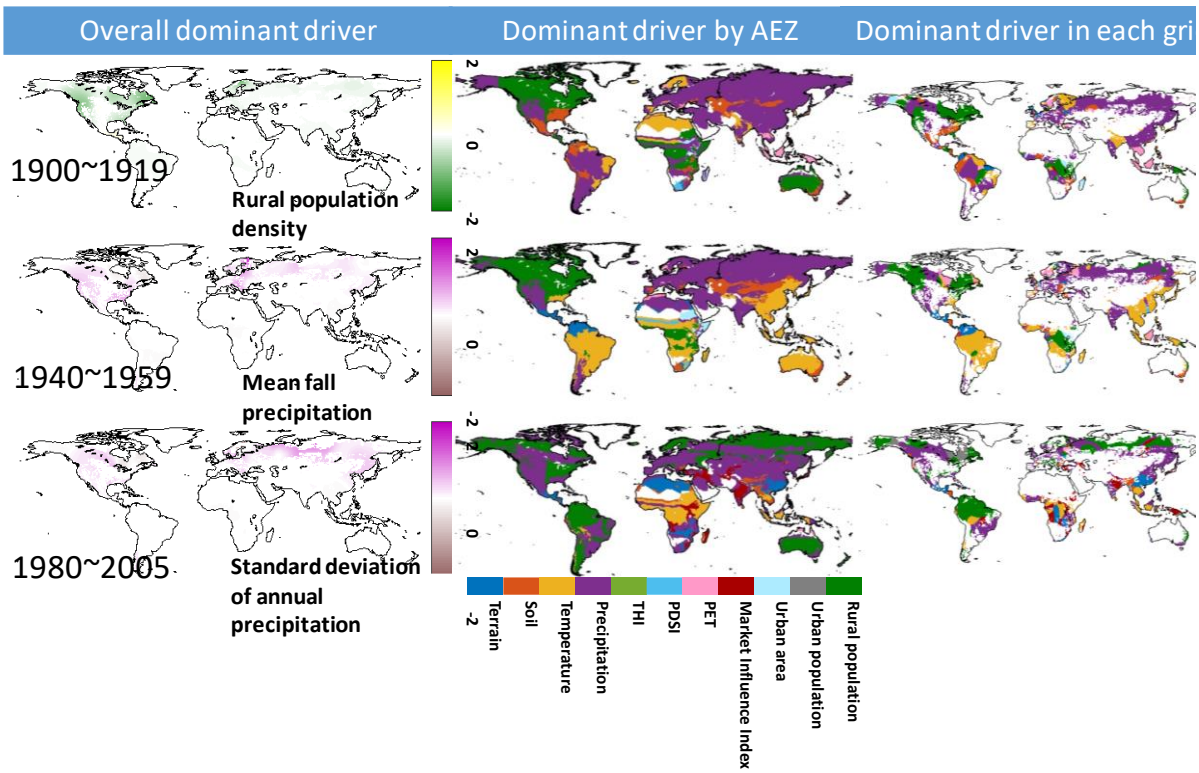

Fig. 5. The dominant drivers of primary forest to the secondary forest are dominant drivers for different

Drivers for the Conversions of Cropland to Secondary Forest. The first column in Figure 6 showed that in 1900 - 1919 and 1980 - 2005, mean spring precipitation and mean fall precipitation were the most dominant drivers for converting cropland to secondary forest. The coefficients in these two periods were mostly positive, indicating that the cropland area to the secondary forest was also bigger in the regions with greater mean spring and fall precipitation. Greater precipitation was beneficial for forest regrowth. Therefore, the area of cropland to the secondary forest would also be bigger in these periods. In 1940 – 1959, spring PET was the most important driver with a positive correlation with the area of cropland conversion to secondary forest.

The second and third columns showed that precipitation, rural population, and PET were the most widespread drivers. The regions with precipitation and PET as dominant drivers intermixed in Eurasia and most of Africa. The rural population was the dominant driver in the western part of North America and some regions in South America. Australia was mainly driven by precipitation. We could conclude that biophysical factors mainly drove the conversion from cropland to the secondary forest except in the western part of North America and the Northwest part of South America in the recent period.

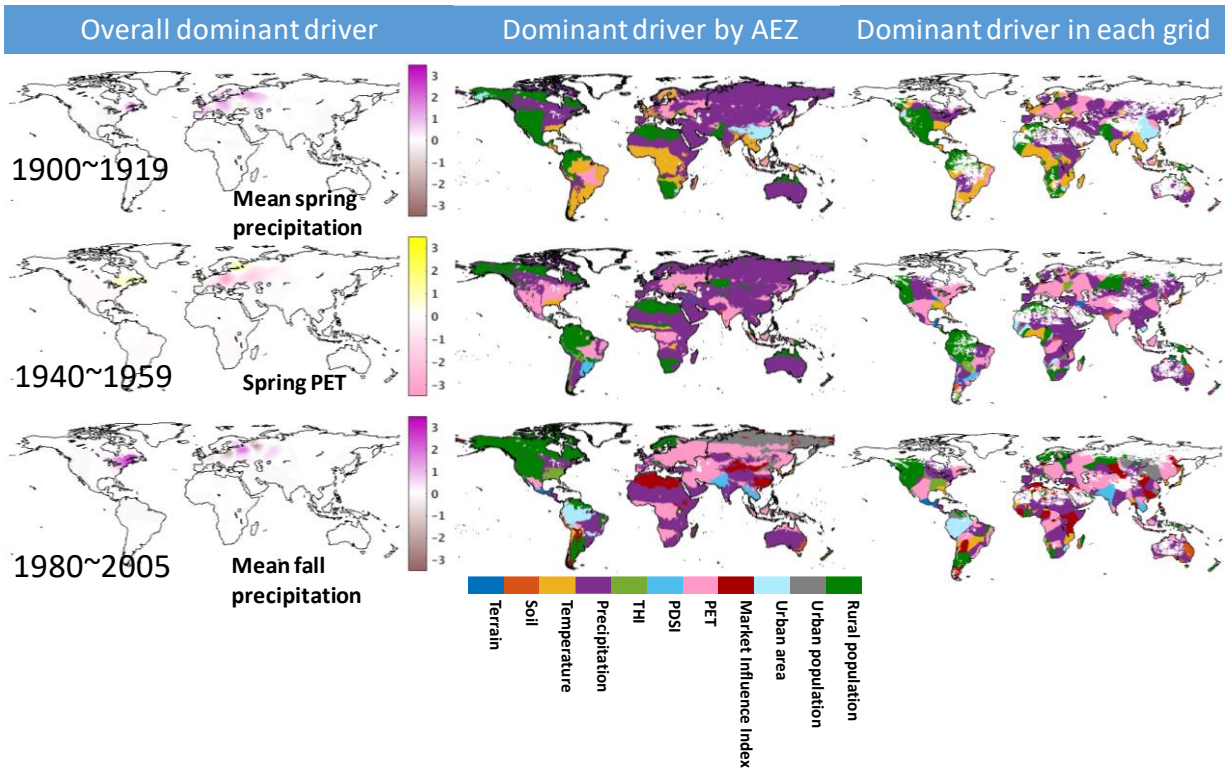

Fig. 6. The dominant drivers of cropland to the secondary forest are dominant drivers for different AEZs and in each grid cell.

Task 1.2. Improving the Historical Distribution of LULCC

We incorporated the abovementioned LULCC drivers at the country- and regional scale to the global LULCC estimate.

Here we briefly describe first the historical downscaling result for crop and pastureland on a global scale. Fig. 7 is an example in the year 2015 demonstrating the differences in cropland and pastureland between our ISAM LULCC data and LUH2. The most apparent differences of the ISAM and LUH2 LULCC data are observed in the forest area. There are ~29 million km^2 forests as estimated in ISAM. By contrast, the forest area is estimated as ~47 million km^2 in LUH2 data.

One reason for this great discrepancy between the two products is the different definitions. ISAM follows the International Geosphere-Biosphere Programme (IGBP) forest definition, which is land dominated by trees with a cover

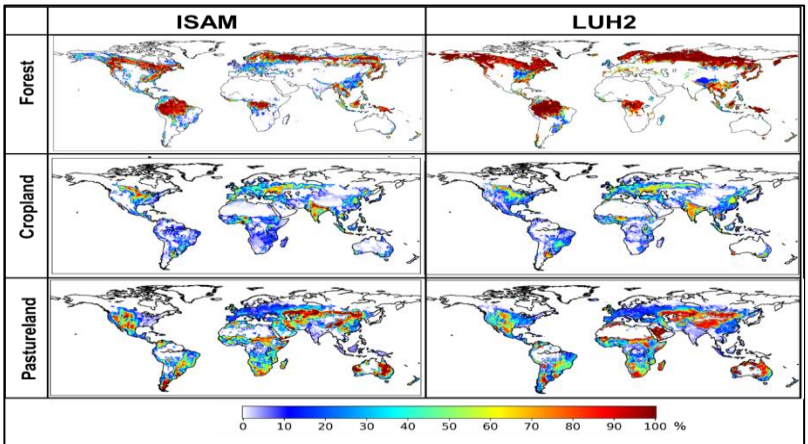

Fig. 7. The cropland and pastureland distribution of ISAM and LUH2 in

of>60% and height exceeding 2 meters. In addition, we have used the Moderate Resolution Imaging Spectroradiometer (MODIS) Collection 5 land-cover data to calibrate the ISAM forest area. The LUH2 forest is the combination of the primary forested land and potentially forested secondary land. Primary land is defined as natural vegetation (either forest or non-forest) that human activities have never impacted. Secondary land is also natural vegetation (either forest or non-forest) that is recovering from previous human disturbance (either wood harvesting or agricultural abandonment).

Task 2: Implementation of Global-Scale Spatial Dynamic Allocation Model (SDAM) in GCAM-E3SM Modeling Framework

Objective and Approach: As originally proposed, our objective under this task is to implement SDAM of agricultural land-use change in the GCAM-E3SM model framework. The SDAM specifically downscales agricultural (cropland and pastureland) land use to the grid cell level from large world regions. To accomplish this task, we applied the SDAM driven by nonlinear interactions between (1) historical and future socioeconomic conditions (e.g., population and economy), (2) biophysical characteristics of the land (e.g., soil, topography, and climate), (3) land use based on the base map of 10 years ago (lag year), and (4) the model parameter estimations for 32 geopolitical regions to match the GCAM regions. Note that the original SDAM considered only nine geopolitical regions.

Task 2.1. Improvement of the spatial autocorrelation function of the SDAM model

The SDAM estimates of land use changes within each grid cell are driven by the maximum profit, spatial and temporal autocorrelation, and the nonlinear impacts from socioeconomic conditions (e.g. population and economy) and biophysical characteristics of the land (e.g., soil, topography, and climate). We used the updated SDAM to downscale the historical (1900-2005) and future (2006-2100 under scenario SSP4-6.0, developed by GCAM modeling framework) agricultural land use (cropland and pastureland) in combination with the following input information: biophysical and socioeconomic variables for historical time and for the future scenario, historical and future cropland and pastureland demands.

Model Improvement

In order to adapt the GCAM-E3SM model framework, we have improved the spatial autocorrelation function. In the original version of SDAM, the spatial autocorrelation function is a scalar factor of the dynamic function together with another adjusted scalar. Our proposed SDAM could reflect complicated nonlinear interactions of socioeconomic conditions and biophysical characteristics of the land and their impacts on LULCC. Such socioeconomic and biophysical variables can reflect the suitability of the land for certain land-use types. We consider the spatial autocorrelation function also reflects the suitability of a grid cell. For example, if a grid cell's neighbors have higher fractions of cropland, this grid cell is more suitable for cropland. The spatial autocorrelation scalar should be in the static function part of the model. The improved model framework can be expressed as the following equation.

$$Min\ (Y^t - Y^{\bar{t}})' A (Y^t - Y^{\bar{t}}) + (Y^t - DS^t - B)'(Y^t - DS^t - B) \quad \text{(Eq. 1)}$$

Therefore, the cropland and pastureland fraction Y^t at time step *t* can be calculated as

$$Y^t = \frac{AY^{\bar{t}} + B + DS^t}{A+1} \quad \text{(Eq. 2)}$$

Where, $Y^{\bar{t}}$ is the cropland and pastureland fraction at previous time step $\bar{t}$, A is the adjustment coefficient, B is the spatial autocorrelation coefficient, D is the managed land fraction, the logits for S^t splits the managed land fraction into proportions of cropland and pastureland.

Parameter Estimation

The original version of the SDAM downscaled the agricultural land use in nine regions across the globe. We extended the model to 32 geopolitical regions to match the GCAM regions. We estimated the parameters in each of the 32 regions. We used the historical RF data and the CRU-TS 3.2 climate data, and other biophysical and socioeconomic variables to estimate the parameters of SDAM. The SDAM model parameter estimating approach remains the same as Meiyappan et al. (2014).

Five Shared Socioeconomic Pathways (SSPs) have been developed, spanning a range of challenges to mitigation and challenges to adaptation. The Shared Socioeconomic Pathway 4 (SSP4), "Inequality" or "A Road Divided," is one of these scenarios, characterized by low challenges to mitigation and high challenges to adaptation. GCAM is chosen as the marker model for this scenario. This task has downscaled the cropland and pastureland from GCAM simulations at a regional scale to 0.5 x 0.5 degree grid-level under two GCAM simulated scenarios: SSP4-6.0 and SSP4-3.4.

Task 2.2. Downscale GCAM simulated agricultural land under SSP4-6.0

Downscaling results

Here we presented the downscaling results from 2020 to 2100 (Fig. 8).

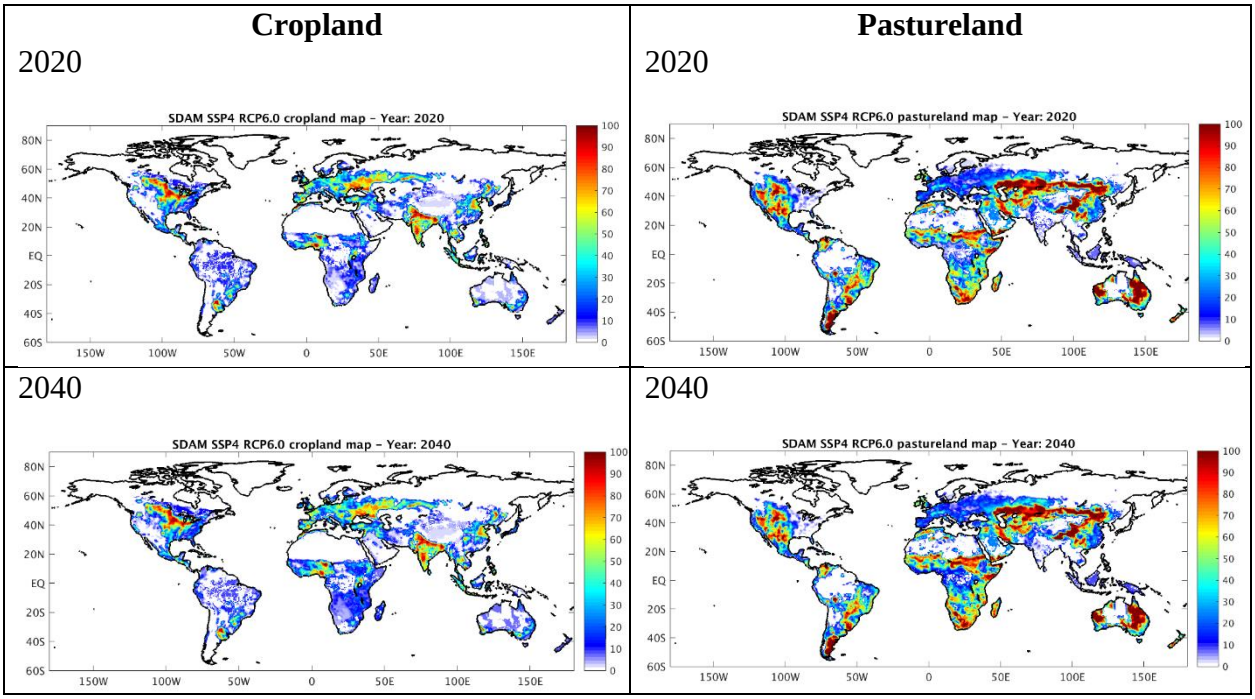

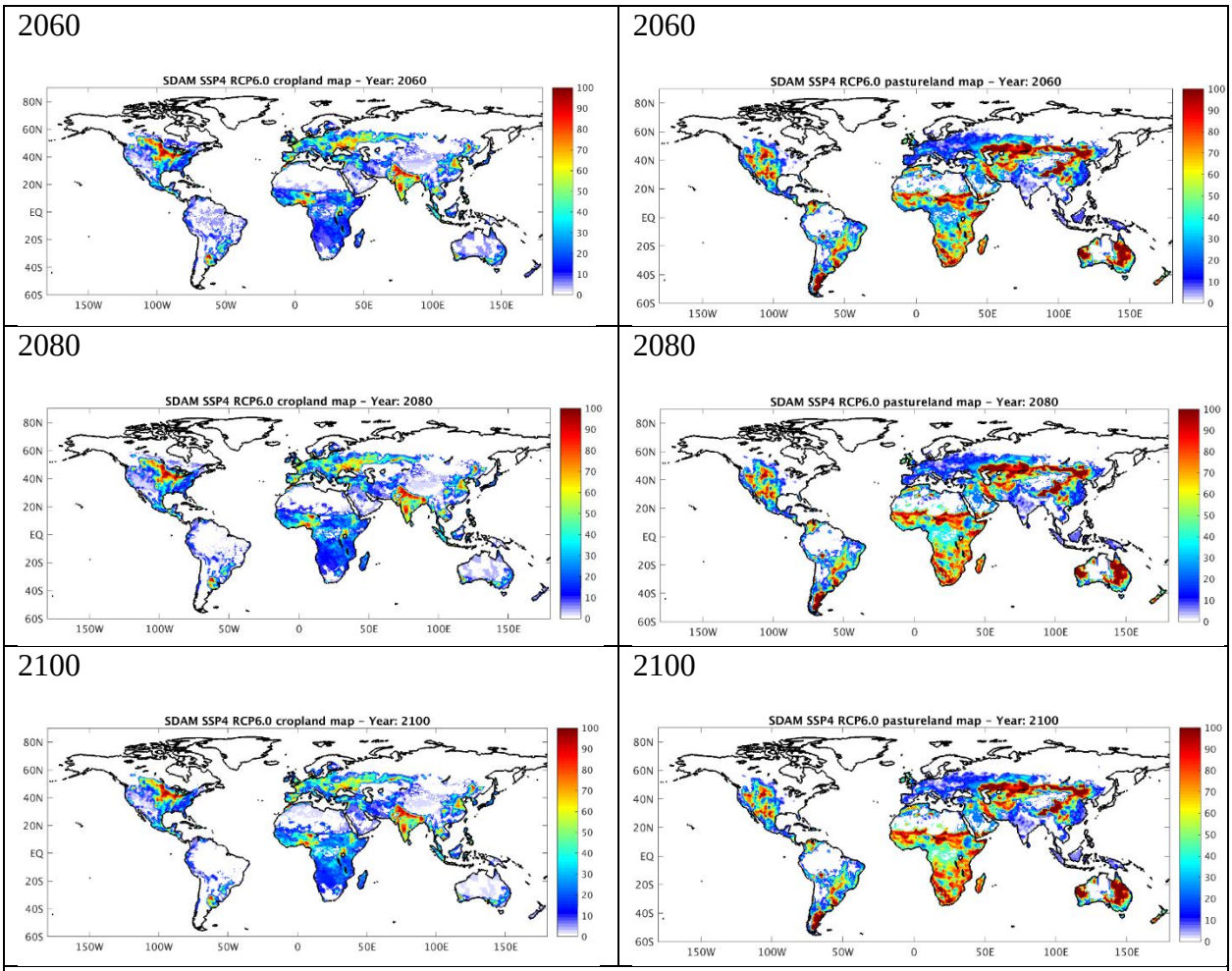

Fig. 8. Downscaled cropland and pastureland maps (Unit: %) for years 2020, 2040, 2060, 2080 and 2100 using SDAM under SSP4-6.0

Comparing the above figures, we could find that the cropland distribution in many regions will not change significantly, such as North and South America, Europe, India, Australia. By contrast, cropland in Sub-Saharan Africa is predicted to change significantly. In Sub-Saharan Africa, the most significant changes occurred in central Africa. This region did not have much cropland distribution at the beginning of the 21st century, but is predicted to be a concentrated region at the end of the century. In the case of the pastureland, the most significant change was observed in Sub-Saharan Africa. The spatial extent remained similar in different years. However, the proportion of pastureland in this region is predicted to increase tremendously by 2100.

Impacts of population and economy on agricultural land

Fig. 9 suggests that Sub-Saharan Africa and China would be the hotspot region of agricultural LULCC under SSP4-6.0. Fig. 3 showed the areas of cropland and pastureland in these regions, including Africa Eastern, Africa Southern, Africa Western, and China according to the GCAM simulation under SSP4-6.0 (Fig. 10).

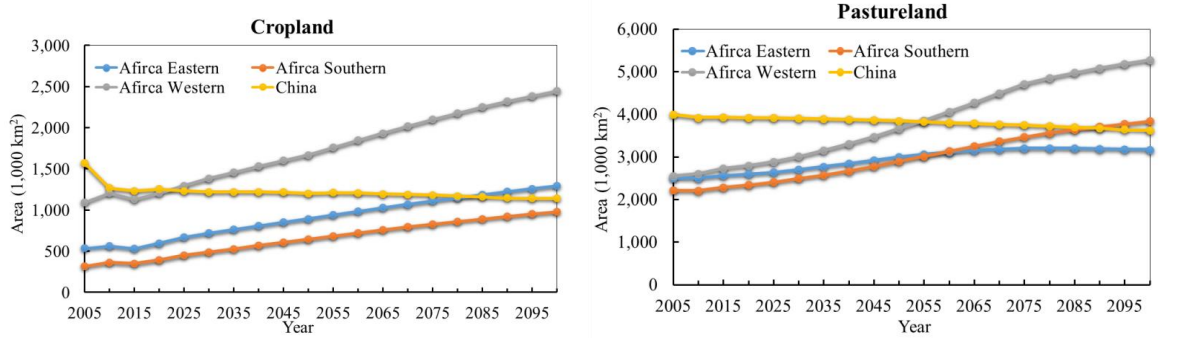

Fig. 9. Cropland and pastureland areas in 21st century produced by GCAM in selected regions under SSP4-6.0

As predicted by GCAM under SSP4-6.0, both cropland and pastureland will increase considerably in Eastern, Southern, and Western Africa, while a large area of cropland and pastureland will decrease in China in the 21st century. These changes led to the variations in spatial patterns in our SDAM simulations. The changes in cropland and pastureland were related to the population and economic factors. Therefore, we showed the population and GDP of these regions in Fig. 10.

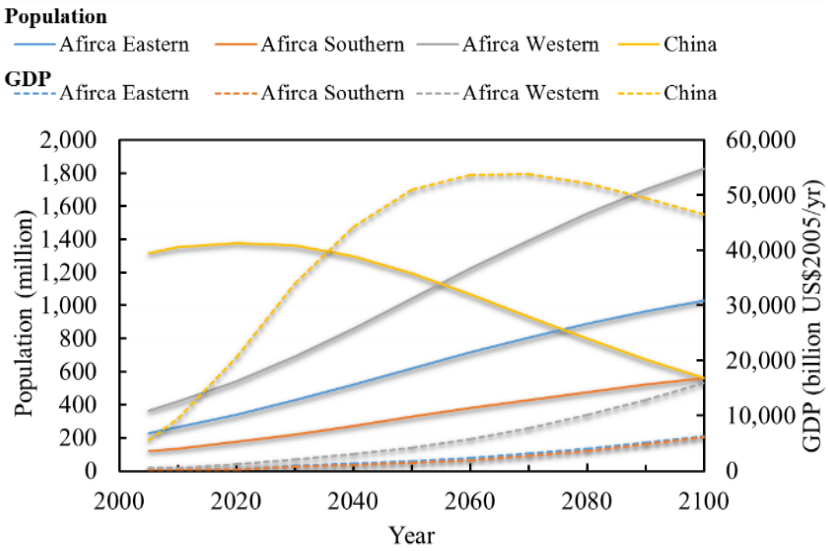

Fig. 10. Population and GDP in 21st century produced by GCAM in selected regions under SSP4-6.0

As shown in Fig.10, Africa Eastern, and Africa Southern, Africa Western will experience rapid increases in both population and economy under the SSP4-6.0 scenario. The increasing population and GDP demand more cropland and pastureland, resulting in the significant changes in both cropland and pastureland in the future. By contrast, the population of China will decrease from 1,315 million in 2005 to 562 million in 2100, according to the simulation. GDP of China will decrease starting at ~2070. These changes lead to less demand on both cropland and pastureland in China. Therefore, the SDAM simulated an expanding trend in Sub-Saharan Africa and a shrinking trend in China for cropland and pastureland. These changing trends originated from the socioeconomic condition under the storyline of the SSP4-6.0 scenario.

Task 2.3. Downscale GCAM simulated agricultural land under SSP4-3.4 and comparison with other global LULCC datasets

LULCC patterns of SDAM, Demeter and LUH2

Here we show the SDAM downscaling results and the comparison with the other two global LULCC datasets, Demeter and LUH2, in the year 2100, end of the simulation period (Fig. 11).

Fig. 11 shows that Demeter and LUH2 estimate the same or similar spatial patterns of cropland, pastureland, and forest in 2100, while SDAM simulates a different pattern. For cropland, we can observe that over India, both Demeter and LUH2 are simulating a more homogenous distribution in most countries. By contrast, SDAM has captured a more heterogeneous distribution in India. Another example is that SDAM has simulated a higher cropland fraction in the Midwest than Demeter and LUH2.

Three datasets have large differences in pastureland distribution, especially in Sub-Saharan Africa, Central Asia, and the Middle East. In Sub-Saharan Africa, the pastureland distribution is more concentrated in Demeter, SDAM, and LUH2 both show heterogeneous distributions. In Central Asia and the Middle East, SDAM has simulated relatively small fractions of pastureland, while Demeter and LUH2 estimate a higher pastureland percentage.

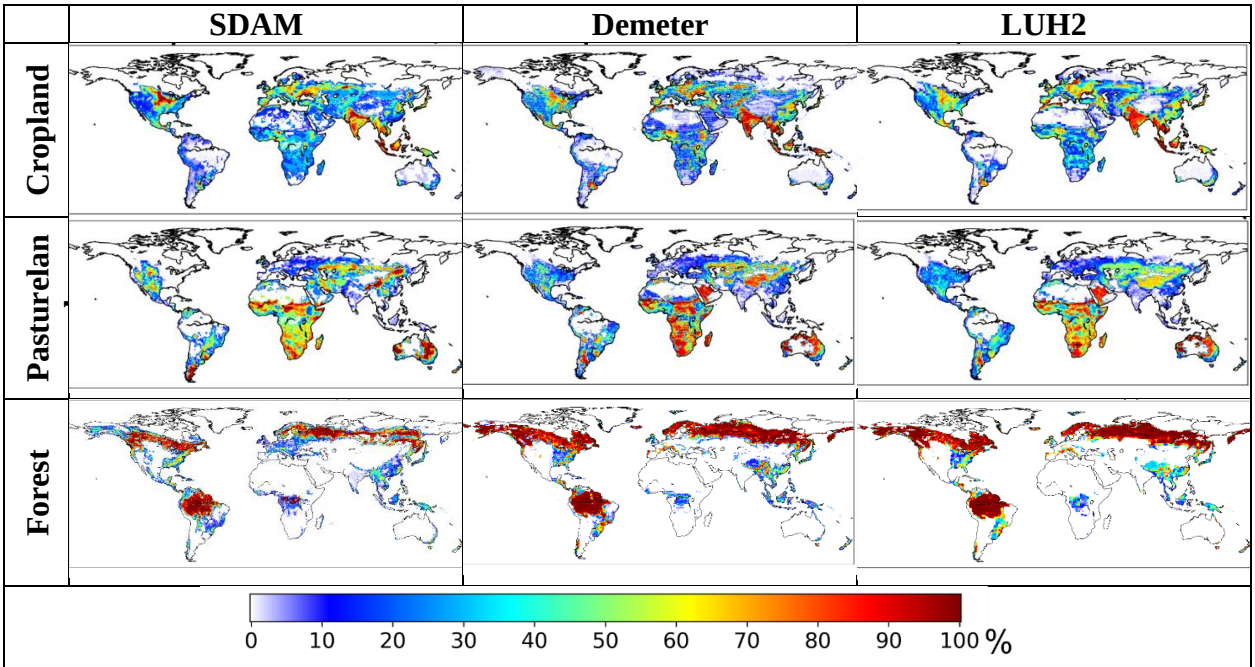

Fig. 11. SDAM downscaled cropland, pastureland and forest maps under SSP4-3.4 for years 2100 and comparison with Demeter and LUH2

Similar to the comparison of LUH2 and ISAM historical LULCC data, the most significant difference of the three datasets is observed in forests, especially in the northern high latitude (NHL) regions. Demeter and LUH2 have estimated a higher forest coverage in NHL, while ISAM follows the present forest distribution (2015) and shows a relatively lower forest fraction in these regions. The areas of forest in these three products are largely different (Fig. 6). Demeter and LUH2 estimated a similar forest area of about ~32 million km^2, while SDAM has estimated a much lower forest area of ~23 million km^2. Fig. 6 also demonstrates that this difference has been inherited from the present time to the future.

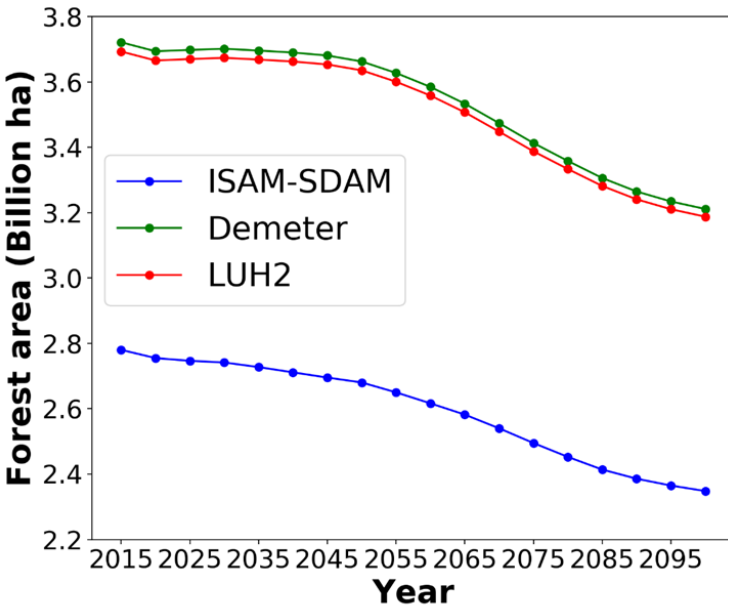

Fig. 12. Forest area of SDAM, Demeter and LUH2 in 21st century under SSP4-3.4

Forest changing trend of three products

Despite the differences in the magnitude of the forest area of these three products, the changing trends are similar. Here we investigate the changing trends of the forest fraction in each grid cell of the three products from 2015 to 2100. Fig. 13 demonstrates the increasing or decreasing trend of the forest of three individual products.

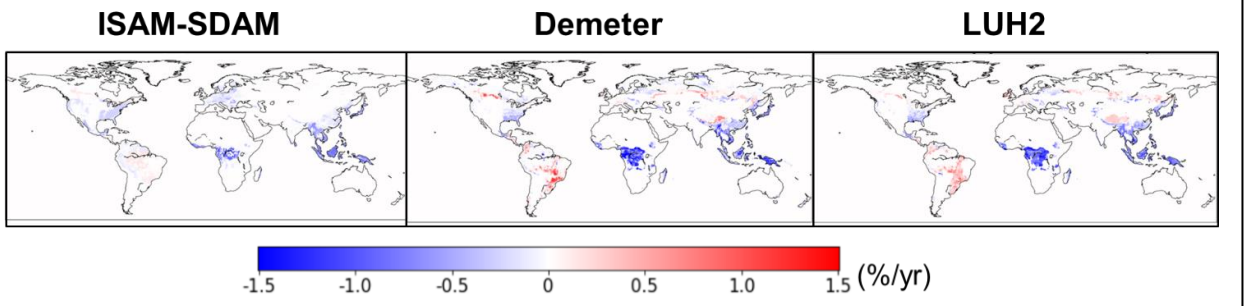

Fig. 13. Forest changing trend between 2015 and 2100 ($p<0.05$)

We have further overlaid these three changing trend maps to detect the grid cells with the same changing trends (Fig. 14). The results suggest that the changing trend of forests over 2015 – 2100 are similar among the three products, although the rates are different. Overall, the forest is projected to decrease in the eastern US, Eastern China, Central Africa, and Southeast Asia in this century. Meanwhile, forest area will increase in Brazil and a few scattered spots in NHL regions.

Impacts of biophysical and socioeconomic factors on forest differences of three products

In order to study the relationships between different biophysical and socioeconomic factors on the differences of three products, we have used stepwise regression to estimate the factors that have contributed to this divergence.

As the first step, we estimate the standard deviation of the forest fraction at each grid cell among three products, which will be the dependent variable of the stepwise regression (Fig. 15).

The explanatory variables, or the independent variables of the regression, are compiled from 46 biophysical and socioeconomic factors at 0.5 x 0.5 degree resolution. In each step of the stepwise regression, an explanatory variable is added, all candidate variables in the model are checked to see if their significance has been reduced below the specified tolerance level. If a non-significant variable is found, this explanatory variable is removed from the model. Because we have standardized all explanatory variables prior to the regression to the same scale, the regression coefficient of each explanatory variable can indicate the relative importance of these variables to the differences among the three products. We have shown the ten most important factors that

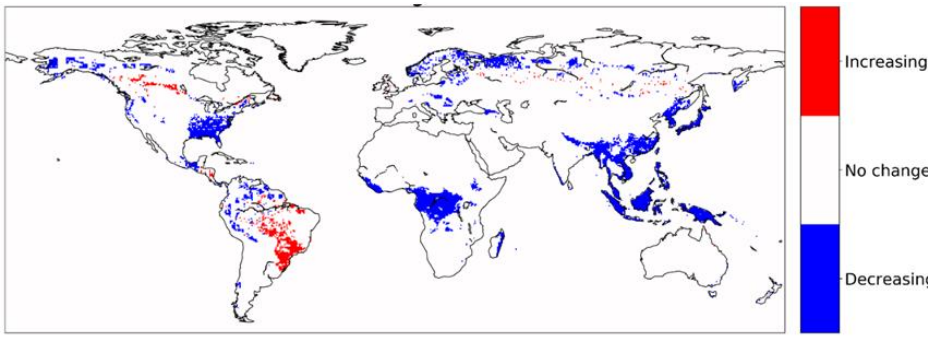

Fig. 14. Same changing trend of forest area among three products

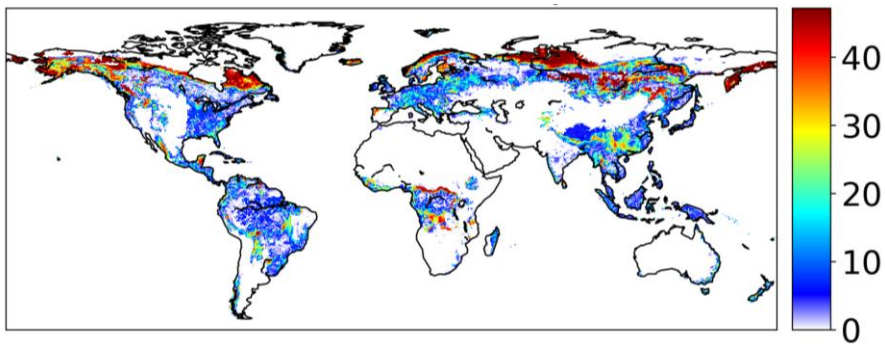

Fig. 15. Standard deviation of forest fraction in three products in 2015 (%)

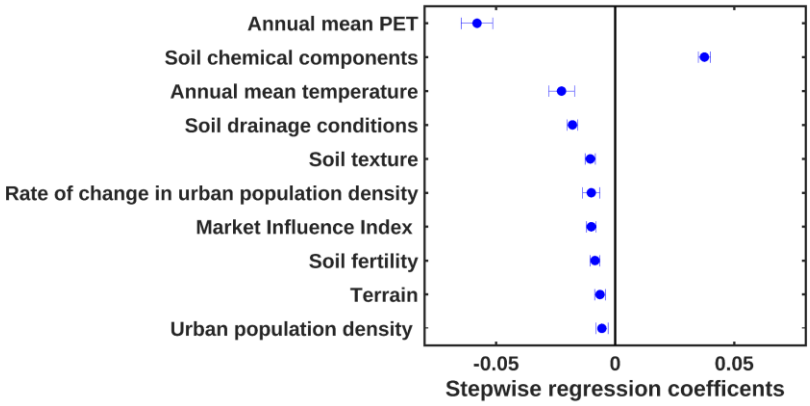

Fig. 16. Ten most important explanatory variables contributing to the differences of forest fraction in three products

have contributed to the forest differences in the three products (Fig. 16).

The results indicate that the forest area differences are more likely to be great in the regions with lower PET and temperature, less fertile, coarser texture, better chemical condition (for agriculture) soil, lower and flatter terrain, and less human activities. Such regions are mostly located in the NHL.

Task 2.4. Responses of the carbon, energy, and water fluxes to different LULCC products in the E3SM model

In this sub-task, we studied the impacts of LULCC on biogeochemistry and biogeophysics using the E3SM model or its land model (ELM). In particular, we compared the E3SM results for soil carbon, GPP and NBP with two different LULCC data: ISAM and LUH2. As a comparison, we also performed simulations using the Integrated Science Assessment Model (ISAM model) with two these two LULCC datasets.

ISAM LULCC data for the ELM simulations

The ELM has defined 16 plant function types, different from the ISAM data with 24 PFTs. In order to drive the ELM with ISAM LULCC data, we first convert the ISAM PFTs to the ELM compatible PFTs as the following table.

Table 2. Correspondence of ELM and ISAM PFT definitions and corresponding areas

	ELM PFT (16)	**ISAM PFT (24)**	**LUH2 area (m^2)**	**ISAM area (m^2)**
1	Wasteland		5.56E+13	3.63E+13
2	Needleleaf evergreen tree – temperate	Primary + secondary temperate evergreen needleleaf forest	5.77E+12	3.46E+12
3	Needleleaf evergreen tree - boreal	Primary + secondary boreal evergreen needleleaf forest	1.09E+13	6.21E+12
4	Needleleaf deciduous tree – boreal	Primary + secondary boreal deciduous needleleaf forest	1.53E+12	2.40E+12
5	Broadleaf evergreen tree – tropical	Primary + secondary tropical evergreen broadleaf forest	1.55E+13	1.46E+13
6	Broadleaf evergreen tree - temperate	Primary + secondary temperate evergreen broadleaf forest	2.55E+12	7.80E+11
7	Broadleaf deciduous tree – tropical	Primary + secondary tropical deciduous broadleaf forest	9.82E+12	3.51E+12
8	Broadleaf deciduous tree – temperate	Primary + secondary temperate deciduous broadleaf forest	6.87E+12	3.67E+12
9	Broadleaf deciduous tree – boreal	-	2.27E+12	0
10	Broadleaf evergreen shrub – temperate	Dense shrubland + open shrubland	7.18E+12	1.49E+13
11	Broadleaf deciduous shrub – temperate	-	2.82E+11	0
12	Broadleaf deciduous shrub – boreal	Dense shrubland + open shrubland	9.03E+12	1.95E+12
13	C3 arctic grass	C3 grassland/steppe + C3 pastureland + Tundra + Savanna	4.83E+12	1.84E+13
14	C3 grass	C3 grassland/steppe + C3 pastureland + Tundra + Savanna	1.55E+13	2.31E+13

15	C4 grass	C4 grassland/steppe + C4 pastureland + Tundra + Savanna	1.29E+13	1.64E+13
16	Crop	C3 cropland + C4 cropland	5.61E+12	5.67E+12

As shown in Table 2, except for needleleaf deciduous tree – boreal, all other forest areas are higher in LUH2 than ISAM. This caused a much higher total forest area in LUH2 than ISAM.

Soil organic carbon pool response to different LULCC datasets

Fig. 17 presents the spatial distribution of soil organic carbon (SOC) pool simulated by two land models (ELM and ISAM) driven by two LULCC datasets: ISAM-SDAM (short as ISAM data hereafter) and LUH2. Despite the large differences in the area of different land use and land cover types (as discussed in Task 1.2), ELM has estimated a similar SOC pool size, which is 1,170 PgC with ISAM data and 1,124 PgC with LUH2 data. The spatial pattern of SOC is also similar between the two datasets, which both show higher SOC density in northern high latitude regions. This indicates that the ELM SOC is not sensitive to the LULCC forcing data. When comparing with the results of ISAM model, we found that the response of the SOC pool is much greater than the ELM model, which estimates the SOC pool as 1,079 PgC and 1,305 PgC when driven by ISAM and LUH2 data sets. ISAM model shows the great response of SOC pool to LULCC forcing.

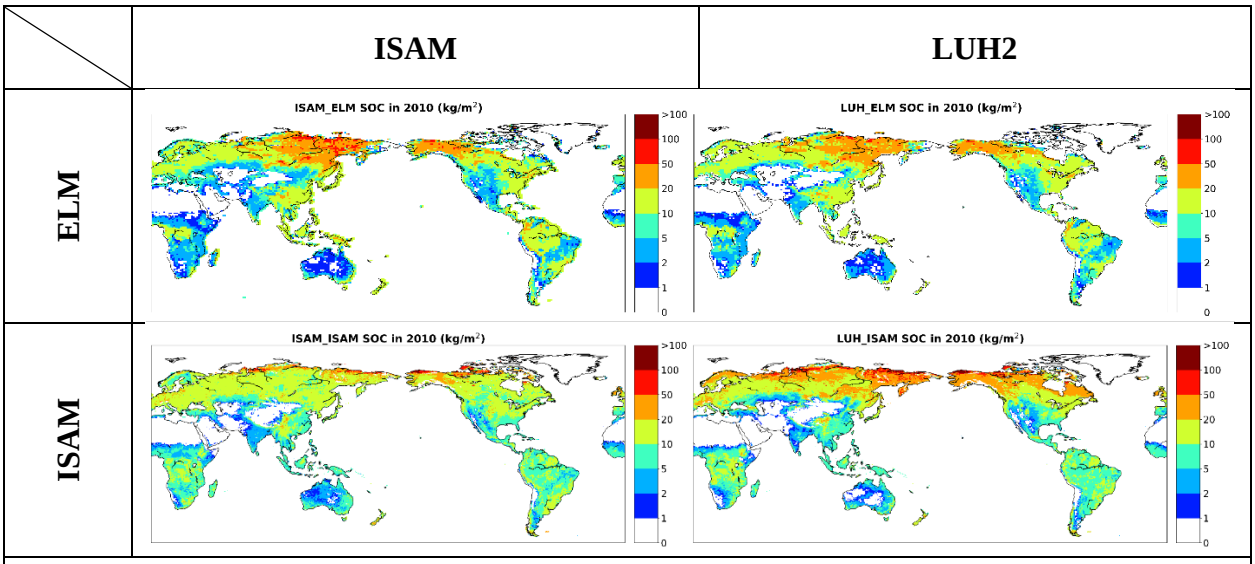

Fig. 17. ELM and ISAM simulated soil organic carbon distribution driven by ISAM and LUH2 LULCC datasets in 2010.

GPP response to different LULCC datasets

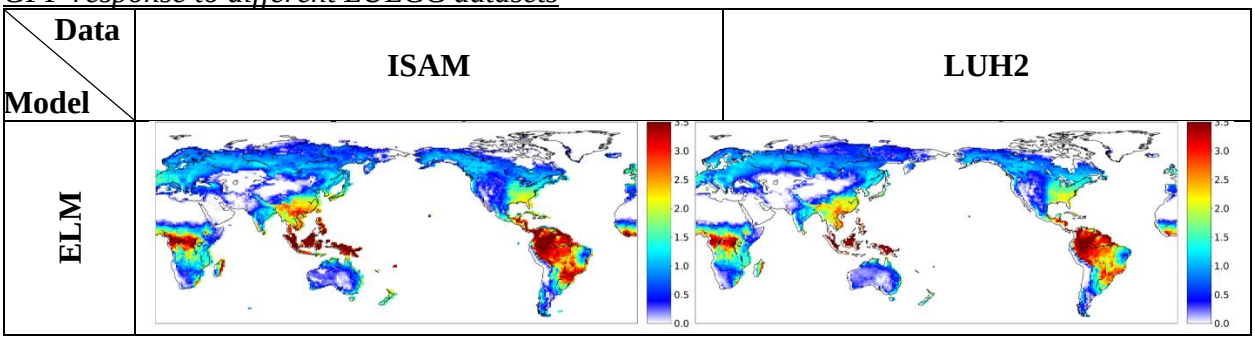

ISAM	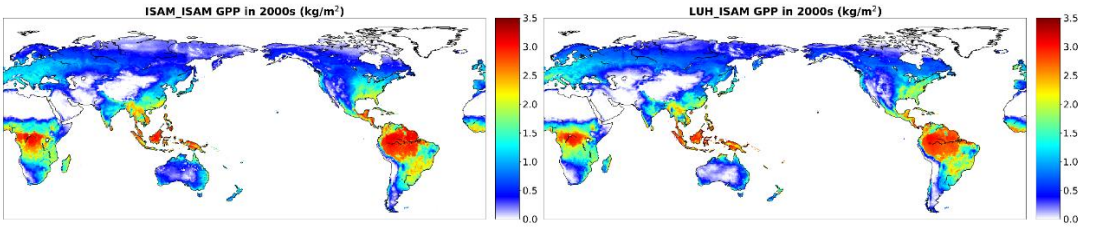

Fig. 18. ELM and ISAM simulated GPP distribution driven by ISAM and LUH2 LULCC datasets in 2010.

GPP spatial patterns are similar in both four cases (Fig. 18). ELM has estimated a global GPP of 140 PgC with ISAM data and 135 PgC with LUH2 data. ISAM model estimates the GPP as 123 PgC and 117 PgC when driven by ISAM data and LUH2 data, respectively. The magnitude of GPP in tropical forests is higher in ELM simulations than in ISAM simulations using both data. The ELM also has estimated a slightly higher GPP in the northern high latitude region.

NBP response to different LULCC datasets

ELM has estimated 0.89 PgC of NBP with ISAM data and 0.77 PgC of NBP with LUH2 (Fig. 19). Both cases are higher than two ISAM model simulations, which are 0.76 PgC with ISAM data, and 0.21 PgC with LUH2 data. Two ELM model simulations show a similar spatial pattern in terms of carbon sink or source. For example, the northern high latitude regions are simulated as a carbon sink, while Southeast Asia and Sub-Saharan Africa are carbon sources. ISAM model simulation with ISAM data shows a similar spatial pattern, but ISAM model with LUH2 data presents a distinct pattern. Unlike other simulations, northern high latitude regions are weak carbon sources.

Data / Model	ISAM	LUH2
ELM	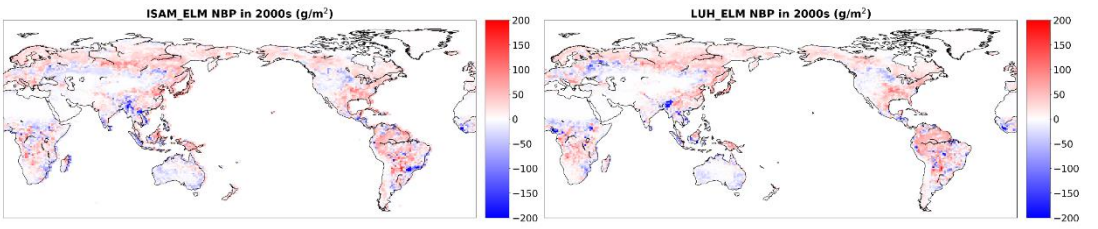	
ISAM	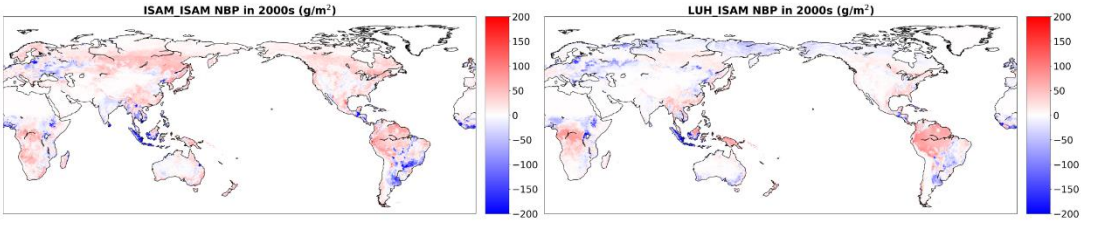	

Fig. 19. ELM and ISAM simulated NBP distribution driven by ISAM and LUH2 LULCC datasets in 2010.

Task 3. Modeling Land Management Practices that Influence Carbon Sinks in Terrestrial Agriculture and Forest Ecosystems and Mitigate Climate Change

Objective and Approach: In this task, we have improved the representations of several essential land management practices into the model, such as plowing the soil, planting crops, fertilization, irrigation, harvesting grains, and recovering crop residues. Primarily, we have implemented the livestock system feed–manure cycle into the land surface model to estimate its impact on net carbon fluxes.

Task 3.1. Land management processes

Harvest and residual treatment process

The harvest is calculated at crop-specific harvest day read as input data. The crop-specific harvest index (HI) and root to shoot ratio (RS) developed by Pacific Northwest National Laboratory (PNNL) is used for the harvest process, which takes place in three steps. In the first step, we compare ISAM simulated and data for root to shoot ratio for all crops. If there is a significant difference between the two, we adjust the above-ground and below-ground biomass based on the reported root to shoot ratio. The above-ground biomass is harvested based on the harvest index for the individual crop in the second step. In the third step, a part of the residual from above ground is treated as recovered residual (i.e., straw, stover) based on the individual crop's recovery rate. The crop grain biomass and the recovered biomass for livestock feed and other socioeconomics uses are assumed to be released into the atmosphere within one year. After harvest and recovery, a certain fraction (in different regions) of the remaining residue is burned on the ground. After harvesting, recovering and burning, the remaining residue biomass goes into the soil in the form of litterfall.

Tillage process

Tillage is a common practice followed by farmers to prepare the land for crop production (i.e., seeding, weed control). During this process, the soil's top layer is disturbed and releases the carbon stored in the soil into the atmosphere. ISAM model assumes that all fresh carbon input accumulated in the crop growing season in the top 20 cm soils will be lost during the tillage process. Part of the lost carbon is emitted into the atmosphere, and part of it is transported into the deeper layer of soil.

Manure C and N treatment

We considered nitrogen and carbon from manure in this study. Manure was either left on the grazing land or collected in the feedlot and then applied to cropland and grazing land.

The crop-specific spatial data of manure nitrogen application amount for cropland was estimated in our produced N fertilizer application amount based on published datasets. For grazing land, we used the gridded nitrogen inputs for circa 2010, which provided manure nitrogen left and applied to grazing land separately.

These crop and grazing land manure nitrogen data were at a gridded scale that was required by the ISAM simulations. The nitrogen datasets were all based on and consistent with FAOSTAT manure nitrogen data at the country scale. Therefore, our usage of FAOSTAT manure management emissions was also consistent with these manure nitrogen input data. Manure contained both organic and mineral nitrogen. Plants could not directly use organic nitrogen. In ISAM model, the

organic manure nitrogen was gradually decomposed by soil microbes to mineral nitrogen. Part of it then entered into the soil mineral nitrogen pool together with the inorganic (mineral) manure nitrogen.

To obtain the spatial data for manure carbon, we first estimated the total manure carbon amount by multiplying the animal-specific manure production per head with live animal heads in different countries. Then we calculated the global total manure nitrogen (estimated in the last paragraph) and determined the global average C:N ratio of manure. Note that the different manure C and N sources might introduce an inconsistency in the global manure C:N ratio estimation. We multiplied this C:N ratio with the spatial maps of manure nitrogen to get the gridded manure carbon map on a global scale. ISAM considered manure carbon in organic form as litterfall and simulated its impact on farmland CO_2 emissions through dynamic processes.

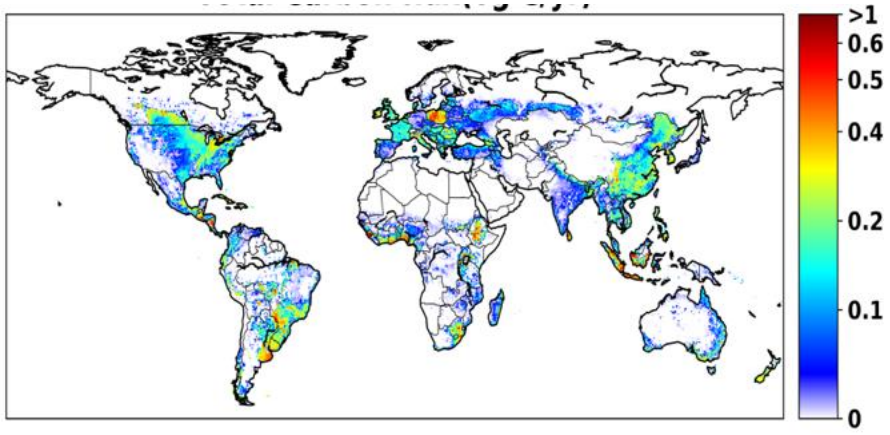

Fig. 20. Global net carbon flux at spatial distribution at 0.5 x 0.5 resolution

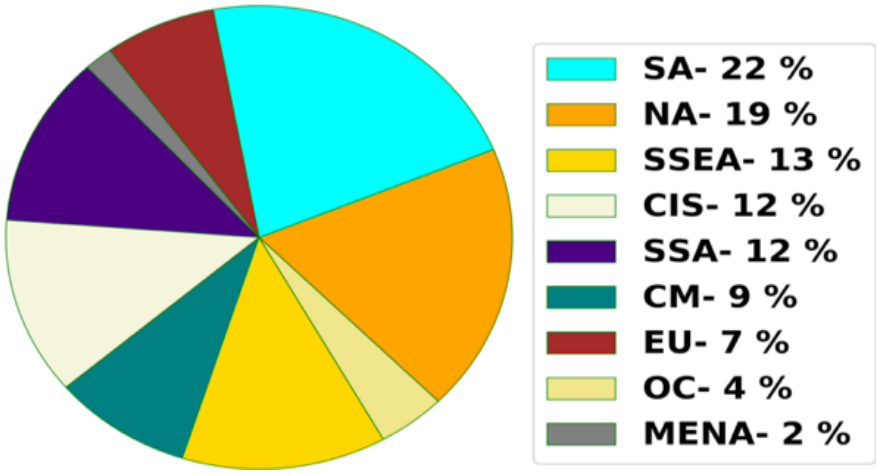

Fig. 21. Net carbon flux in different regions. Percentage contribution for each region to the total flux and actual values for each region. (NA: North America, SA: South America, EU: European Union, MENA: Mid East and North Africa, SSA: Sub-Saharan Africa, CIS: Commonwealth of Independent States, CM: China and Mongolia, SSEA: South and Southeast Asia, OC: Oceania and other East Asia)

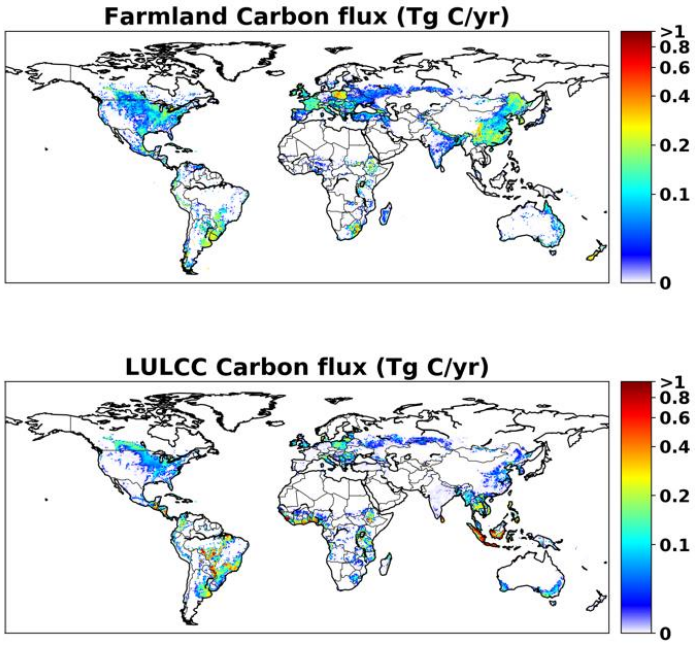

Fig. 22. Global net carbon flux due to land-use change (E_{luc}) and farmland activities (E_{farm}).

Irrigation process

The irrigation amount (W_{irrig}) is estimated as the soil moisture deficit between irrigation target (W_t) and soil water content (W_{liq}) within the root-zone as follows:

$$Wirrg = W_t - W_{liq} \qquad \text{(Eq 3)}$$

where W_t is considered as a soil moisture content with no water stress (i.e., WS is 1.0) for crop photosynthesis during the growing period.

Task 3.2. Estimate the carbon fluxes due to agricultural land management and LULCC

This study estimated global total net carbon flux from agricultural land is 2.26 Pg C/yr. Our study suggests agricultural land to be a net source of carbon globally. At the spatial scale, the hot spot areas for carbon emissions lie within the countries like Brazil, Argentina, Ethiopia, and Indonesia (Fig. 20). Within the nine macro-geographical regions**,** South America (SA, 22%), North America (NA, 19%), and South and Southeast Asia (SSEA, 13%) are the top contributing regions for total net flux. The least contributing regions include Oceanic and other East Asia (OC, 4%), and Mid East and North Africa (MENA, 2%) (Fig. 21).

LUC and Farmland Carbon Fluxes

Farmland (E_{farm}) activities contribute 0.85 Pg C/yr (38%), and LUC (E_{luc}) activities related to agricultural-land expansion contribute 1.41 Pg C/yr (62%) to the total net carbon flux at the global scale. Total E_{luc} is estimated as 5186 Tg CO_2 /yr, which is consistent with the SRCCL (4900 ± 2500 Tg CO_2 /yr) , and the global carbon budget 2019 estimates (5500 ± 2500 Tg CO_2 /yr). A distinct difference between the areas contributing to emissions due to land-use and farmland activities can be seen at the spatial scale. A significant contribution to the total E_{luc} emissions is coming from tropical regions due to higher LUC activities within these regions. On the other hand, the major contributing areas for E_{farm} fluxes lie within temperate regions (Fig. 22).

According to our estimation for regions (Fig. 23), SA and SSEA are the top contributing regions for the LUC activities and contributing 29% and 21% of the total E_{luc}, respectively. In SA, pasture land expansion in favor of cattle ranching has been identified as a significant reason for tropical deforestation. Also, the tropical area in Southeast Asia had the highest deforestation rate globally; the majority of the regions where high deforestation happened were due to cropland expansion. Whereas, for the E_{farm}, NA has the highest contribution of 31%, followed by CIS with 19%.

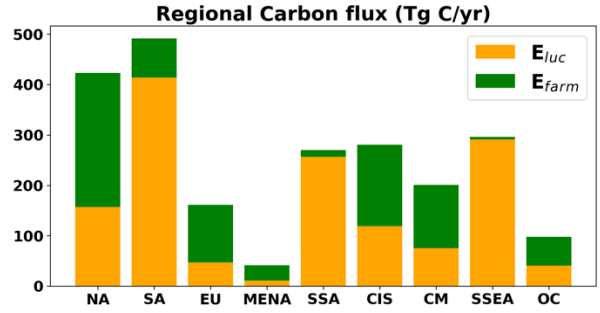

Fig. 23. Net carbon flux due to land-use change (E_{luc}) and farmland activities (E_{farm}) in different regions.

Cropland and Grazing Land Emissions

Cropland is the major contributor with a net carbon flux of 1.63 PgC, compared to cropland, grazing land net carbon flux is less, 0.63 Pg C/yr, accounting for 72% and 28% of net carbon flux from agricultural land, respectively. As discussed above, total emissions produced due to agricultural-land expansion is 1.41 Pg C/yr, of which cropland and grazing land expansion contribute 1.26 Pg C/yr (90%), .15 Pg C/yr (10%), respectively. Whereas farmland activities from cropland and grazing contribute 0.37 Pg C/yr (42%), 0.48 Pg C/yr (57%) to the total E_{farm} of 0.85 Pg C/yr at a global scale, respectively. A major contribution of E_{luc} within cropland is from the South East Asian counties like Indonesia and Malaysia (Fig. 24), where cropland expansion deforestation rates are intense. For grazing land, the estimated E_{farm} is approximately three folds higher than E_{luc} at a global scale, the hot spot region of farmland activities lies within Latin American countries like Brazil and Argentina (Fig. 24).

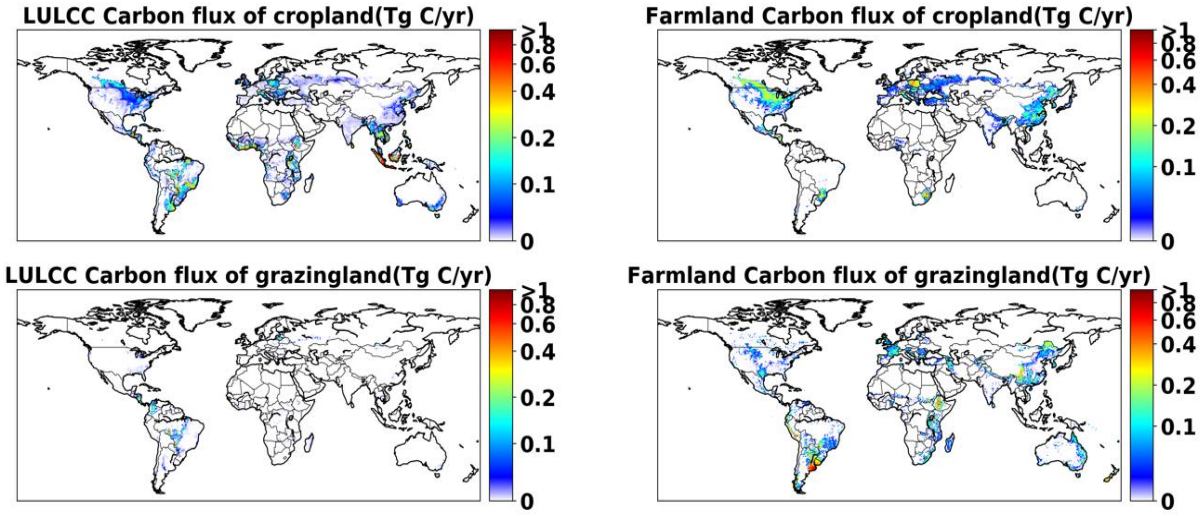

Fig. 24. Global net carbon flux due to land-use change (E_{luc}) and farmland activities (E_{farm}) for cropland and grazing land at 0.5 x 0.5 resolution.

According to our analysis for regions, net flux within cropland and grazing land (Fig. 25), NA (24%), SSEA (17%), Commonwealth of Independent States (CIS, 15%), SA (13%), and China and Mongolia (CM, 13%) are the most prominent regions over the globe. These regions account for the largest share of the world's population, demanding more food and land, driving land-use

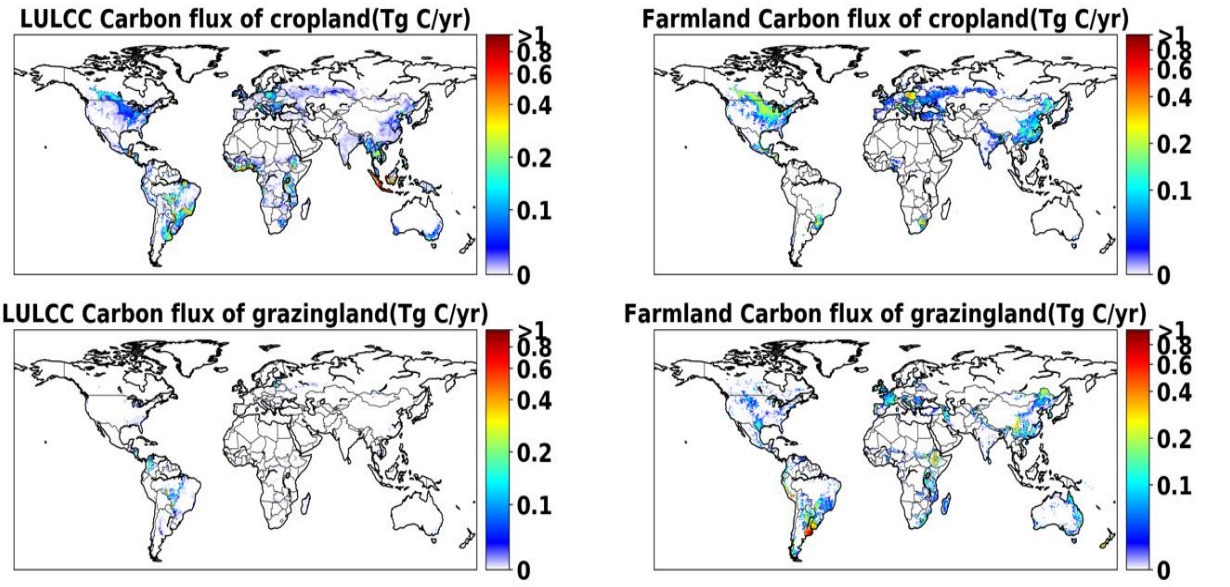

Fig. 25. Net carbon flux from cropland and grazing land in different regions.

change, and intensifying farmland activities, causing more carbon emissions. The most prominent region for net carbon flux within grazing land is SA, which contributes 44% to the total carbon flux produced. The livestock sector in SA has grown at an annual rate of 3.7%, approximately twice compared to the average global growth rate of 2.1%. This boom in livestock production due to an increase in food demand might be the reason for such a high contribution (44%) of the SA region to the total carbon flux in grazing land.

In regards to individual crop contribution, maize, rice, and wheat are the major carbon-emitting crops, contributing 53% of total cropland fluxes, and the net carbon flux from maize is 0.4 PgC/yr (24%), rice 0.26 PgC/yr (16%) and, wheat 0.22 PgC/yr (13%) at the global scale. Maize is dominating in NA (0.09 Pg C/yr) and SA(0.20 Pg C/yr), the wheat highest contribution is coming from NA (0.07 Pg C/yr) and CIS (0.07 Pg C/yr) regions and, rice net flux is highest in SSEA (0.11 Pg C/yr) and CM (0.07 Pg C/yr) regions (Fig. 26). SSEA and CM produce more than 90% of the rice globally and therefore are responsible for the majority of the net carbon flux from rice cultivation. E_{luc} of maize (0.18 Pg C/yr), rice (0.16 Pg C/yr), and wheat (0.12 Pg C/yr) are the highest among all the crops (Fig. 27). Although wheat is majorly cultivated in temperate regions where E_{luc} is less intensive, the largest harvest area still makes its E_{luc} the third largest. The highest E_{farm} is coming from maize is estimated to be 0.21 Pg C/yr, followed by rice and wheat with 0.1 Pg C/yr each.

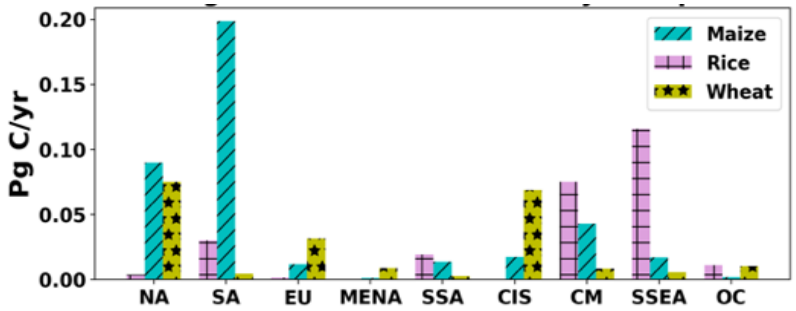

Fig. 26. Net carbon flux from maize, rice, and wheat in different regions.

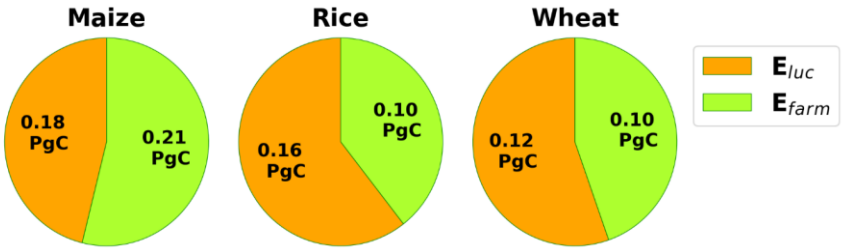

Fig. 27. Global accumulated E_{luc} and E_{farm} for maize, rice, and wheat.

Research papers, Book Chapters, MS and Ph.D. research, and Presentations that have been sponsored completely or in part by DOE program

Research Papers (Total 12 Research Articles)

Teckentrup, L et al. (Coauthor:**AK Jain**) (2021)Assessing the representation of the Australian carbon cycle in global vegetation models, ***Biogeosciences,*** https://doi.org/10.5194/bg-18-5639-2021

Winkler, AJ et al. (Coauthor: **AK Jain**) (2021), Slow-down of the greening trend in natural vegetation with further rise in atmospheric CO2, ***Biogeosciences***, 18, 4985-5010 https://doi.org/10.5194/bg-18-4985-2021

Xu X, Sharma P, Shu S, Lin T, Ciais P, FN Tubiello, P Smith, N Campbell, **AK Jain** (2021). Global greenhouse gas emissions from animal-based foods are twice those of plant-based foods. **Nature Food** 2, 724–732. https://doi.org/10.1038/s43016-021-00358-x

Friedlingstein, P., et al. (Coauthor: **AK Jain**) (2020). Global carbon budget 2020. *Earth System Science Data*, 12(4), 3269-3340. https://doi.org/10.5194/essd-12-3269-2020

Bastos, A., P. Ciais, P. Friedlingstein, S. Sitch, J. Pongratz, L. Fan, J.-P. Wigneron, U. Weber, M. Reichstein, Z. Fu, P. Anthoni, A. Arneth, V. Haverd, **A.K. Jain**, E. Joetzjer, J. Knauer, S. Lienert, T. Loughran, P.C. McGuire, H. Tian, N. Viovy, and S. Zaehle (2020), Direct and seasonal legacy effects of the 2018 heatwave and drought on European ecosystem productivity, *Science Advances*, 6, https://doi.org/10.1126/sciadv.aba2724

Bastos, Z. Fu, P. Ciais, P. Friedlingstein, S. Sitch, J. Pongratz, U. Weber, M. Reichstein, P. Anthoni, A. Arneth, V. Haverd, **A. K. Jain**, E. Joetzjer, J. Knauer, S. Lienert, T. Loughran, P.C. McGuire, W. Obermeier, R.S. Padrón, H. Shi, H. Tian, N. Viovy, and S. Zaehle, "Impacts of extreme summers on European ecosystems: a comparative analysis of 2003, 2010 and 2018, ***Phil. Trans. R. Soc. B***, 375: 20190507, http://dx.doi.org/10.1098/rstb.2019.0507

Xu X, S Shrestha, H Gilani, MK Gumma, BN Siddiqui and **AK Jain** (2020a) Dynamics and Drivers of Land Use and Land Cover Changes in Bangladesh. *Regional Environmental Change*. 2020, 20:54. https://doi.org/10.1007/s10113-020-01650-5

Friedlingstein, P., et al. (Coauthor: **AK Jain**) (2019). Global carbon budget 2019. *Earth System Science Data*, 11(4), 1783-1838. https://doi.org/10.5194/essd-11-1783-2019

Jung, M. et al. (Coauthor: **AK Jain**), (2020), Scaling carbon fluxes from eddy covariance sites to globe: synthesis and evaluation of the FLUXCOM approach, *Biogeosciences*, 17, 1343–1365, 2020, https://doi.org/10.5194/bg-17-1343-2020

Xu X, **AK Jain**, and KV Calvin (2019) Quantify the Biophysical and Socioeconomic Drivers of Changes in Forest and Agricultural Land in South and Southeast Asia. *Global Change Biology*, *25*(6), 2137-2151, https://doi.org/10.1111/gcb.14611

Le Quéré, C., et al. (Coauthor: **AK Jain**) (2018). Global carbon budget 2017. *Earth System Science Data*, 10(1), 405-448, https://doi.org/10.5194/essd-10-405-2018

Le Quéré, C., et al. (Coauthor: **AK Jain**) (2018). Global carbon budget 2018. *Earth System Science Data*, *10*(4), 2141-2194. https://doi.org/10.5194/essd-10-405-2018

Book Chapters (Total 2 Book Chapters)

Jain AK, X Xu and N Hewitt (2019a), Global air pollution problems, In**:** *Handbook of Atmospheric Sciences***,** CN Hewitt and AV Jackson (eds.), Blackwell Science Ltd, Oxford, UK.

Gillani H, F M Qamer, M Sohail, K Uddin, AK Jain and W Ning (2017), Land cover change and its eco-environmental responses in Nepal, In: Review on Ecosystem Monitoring in Nepal and Evolving Earth Observation Technologies (A Li, W Deng, W Zhao (Eds.), Springer Singapore.

Ph.D. Thesis

Shu, Shijie: Quantifying biophysical and biogeochemical influence on northern high latitude greenhouse gases dynamics, Ph.D. Thesis, University of Illinois, Urbana-Champaign, *awarded in July 2021*.

MS Thesis

Eunkyoung, Choi: Modeling the combined environmental effect on net land carbon flux in the present and future scenarios, MS Thesis, University of Illinois, Urbana-Champaign, *awarded in May 2020*.

Sharma, Prateek: Estimation of the global carbon fluxes due to agricultural management activities using a land surface model, MS Thesis, University of Illinois, Urbana-Champaign, *awarded in May 2020*.

Presentation (Total 17 presentations)

Jain, A.K., Xu, X., Shu, S. (2021) Global Carbon Fluxes Induced by Agriculture-Related Land-Use and Land Cover Change Activities. EGU General Assembly Conference. Virtual, April 19-30, 2021.

Xu, X., Jain, A.K., Shu, S., Sharma, P. (2020) Global Carbon Fluxes Induced by Management Practices on Agricultural Land. DOE E3SM All-Hands Meeting. Virtual, October 26-29, 2020.

Jain AK, X Xu, S Shu (2019b) Modeling the Influence of Land Use and Land Cover Change. *Fall E3SM All-Hands Meeting*, Arlington, VA, Nov 19-21, 2019.

Jain AK, X Xu, CC Chen, S Shu, K Calvin, G Bisht, X Yang, D Ricciuto (2018a) Responses of the Carbon, Energy and Water Fluxes to Different Land Use and Land Cover Products in the E3SM Model. *DOE Modeling PI Meeting*, Potomac, MD, Nov 5-9, 2018.

Jain AK and X. Xu (2018), Dynamics and Drivers of Land Cover & Land Use Changes in Bangladesh – Integration of Satellite Data with Socioeconomic Dataset, International meeting Co-Organized by NASA LCLUC program entitled *"Land Cover/Land Use Changes (LC/LUC) and Impacts on Environment in South/Southeast Asia"* - International Regional Science Meeting, Philippines, 28-30th May 2018.

Jain AK (2018), Impacts of Various Environmental Factors and Management Strategies on Food Crops in the South and Southeast Asia (SSEA) Region (2018), International meeting Co-Organized by NASA LCLUC on *Land Use/Cover Change and Water-Energy-Food (WEF) Nexus in Southeast Asia*, Vientiane, LAOS, August 11–17, 2018.

Jain AK (2018), The Impacts of Various Environmental Factors and Management Strategies on Food Crops Over the 21st Century, *Joint Global Research Institute, Pacific Northwest National Laboratory*, College Park, MD, October 22, 2018.

Jain AK (2018), Dynamics and Drivers of Land Use & Land Cover Changes in Bangladesh, the *Intl. Conf. on Advanced Remote Sensing 2018*, Wuhan, China, Oct 16-18, 2018, https://icars2018.sciforum.net/ Keynote Talk

Jain AK (2018), Responses of the Carbon, Energy and Water Fluxes to Different Land Use and Land Cover Products in the E3SM Model, *DOE Modeling Principal Investigators Meeting*, Potomac, MD, Nov 5-9, 2018

Sharma P and AK Jain (2018), Assessing the effects of land use changes, nitrogen fertilizer application on nitrogen leaching in South and South East Asia, American Geophysical Union Fall 2018 Meeting, Washington, DC, 10-114 December 2018.

Xu X, Jain AK, Calvin KV, Chen M, Vernon CR and Huang M (2018a). Comparison between Three Downscaled Land Use and Land Cover Products under Different Shared Socio-Economic Pathways. *American Geophysical Union (AGU) Fall meeting 2018*. Washington DC, USA.

Xu X, AK Jain, and KV Calvin (2018b), Quantify the biophysical and socioeconomic drivers of changes in forest and agricultural land in South and Southeast Asia. *CESM Land Model and Biogeochemistry Working Group Meetings*. 2018. Boulder, CO. 5-8 February 2018.

Jain AK, X Xu, S Shu, K Calvin (2017), Spatiotemporally dynamic drivers of global land use and land cover change in the past century. 2017 All Hands ACME Meeting, Potomac, MD, June 5-7, 2017

Jain AK (2017), Improving the Satellite Derived Forest Cover Dynamics in South and Southeast Asia, Land Cover/Land Use Change, *SARI International Regional Science Meeting in South/Southeast Asia*, Chiang Mai, Thailand, 17-19 July, 2017.

Xu X, AK Jain (2017) Quantify the biophysical and socioeconomic divers of the deforestation/agriculture expansion in South and Southeast Asia, *American Geophysical Union Fall 2017 Meeting*, New Orleans, LA, 11-15 December 2017.

Xu X and AK Jain (2017) Dynamics and Drivers of cropland expansion and forest regrowth in South and Southeast Asia, Land Cover/Land Use Change, *SARI International Regional Science Meeting in South/Southeast Asia*, Chiang Mai, Thailand, 17-19 July, 2017.

Jain AK (2016), Land Cover/Land Use Change Dynamics and Impacts on Carbon and Nitrogen Emissions in South/Southeast Asia, *International Meeting on Land Use and Emissions in South/Southeast Asia*, Ho Chi Minh City, Vietnam, October 17-19th, 2016.